Nonaxisymmetric vesicle shapes in a generalized bilayer-couple model and the transition between oblate and prolate axisymmetric shapes

Volkmar Heinrich,* Saša Svetina, and Boštjan Žekš†
Institute of Biophysics, Medical Faculty, Lipičeva 2, and J. Stefan Institute, University of Ljubljana, SLO-61105 Ljubljana, Slovenia
(Received 12 November 1992)

A theoretical approach to calculate shapes of phospholipid vesicles is developed. It is general in the sense that it is not restricted to shapes with special symmetry properties, and it includes a stability analysis of the shapes. In keeping with recent experimental findings, the description of the vesicle membrane is based on the generalized bilayer-couple model. According to this concept, the bilayer structure of the membrane is modeled by representing its two monolayers as closed neutral surfaces with a constant separation distance. Equilibrium shapes are assumed to correspond to the minimum of the membrane elastic energy at constant values of the membrane area and the vesicle volume. The elastic energy is composed of the local and nonlocal bending energies of the membrane. The latter term represents the energy contribution of the relative area changes of monolayers. The variational problem to calculate equilibrium shapes is solved by applying a Ritz method based on an expansion in spherical harmonics. The numerical computations concentrate on the range of model parameters for which nonaxisymmetric shapes are obtained. In addition, axisymmetric shapes which are obtained in the same range of model parameters are examined. It is shown that small differences of the ratio between the nonlocal and local bending moduli (q) may cause significant changes in the nature of shape transformations. For high q values, nonaxisymmetric shapes are stable, and they represent the intermediate states in the continuous transformation between oblate and prolate axisymmetric shapes. At low q values characteristic for phospholipid bilayers, the nonaxisymmetric shapes are unstable. In this case, the transition between oblate and prolate axisymmetric shapes is discontinuous.

PACS number(s): 87.22.Bt, 62.20.Dc, 02.60.−x

I. INTRODUCTION

Phospholipid vesicles are closed bilayer lipid membranes which form spontaneously in aqueous solutions. Their equilibrium shapes' shape transformations and fluctuations have been a subject of increasing interest in experimental biophysics as well as in theoretical physics [1–4]. The relatively simple vesicle structure enables a detailed experimental investigation of the mechanical properties of membranes and therefore also of related mechanisms taking place in more complex systems such as erythrocytes and other living cells. Several mathematical models have been developed in order to describe the vesicle features theoretically. In some cases, good agreement between experiment and theory has been found so that at least some of the basic mechanisms of shape transformations have been illuminated by theoretical studies [5–14].

The generally accepted basis for the calculation of shapes of phospholipid vesicles is the assumption that equilibrium shapes correspond to the minimum of the membrane elastic energy. The phospholipid bilayer is more or less unstretchable and water impermeable. Accordingly, the constraints of constant vesicle volume and membrane area are usually also part of the basic model assumptions. Two alternative models of vesicle shapes have been proposed and studied: (i) the spontaneous-curvature concept [5–7,9,14], relating shape changes to variations of the spontaneous curvature of the bilayer, and (ii) the bilayer-couple model [10–14], which is based on the bilayer-couple hypothesis [15]. In both models, the only energy contribution taken into consideration is the membrane bending energy.

The bilayer-couple model accounts for the structure of phospholipid membranes by considering the two leaflets of the bilayer separately. While remaining in close contact, both monolayers are assumed to respond to mechanical stresses independently, i.e., they can freely slide over each other in a lateral direction. In general, previous studies of this model have required that both monolayers have constant areas or, more conveniently, that the difference of monolayer areas ΔA be fixed. This model, which includes a "hard" constraint of constant ΔA, will be called in the following the "strict" bilayer-couple model. It enables a suitable classification of equilibrium shapes. A given class comprises all shapes of the same symmetry that are continuously transformed into each other by varying the model parameters, i.e., the relative vesicle volume v and the relative area difference of monolayers Δa [11,16]. Both parameters are normalized with respect to a sphere that has the same surface area as the vesicle. A systematic study of the strict bilayer-couple model revealed that the v-Δa phase diagram comprising axisymmetric shapes of lowest bending energies contains a gap between oblate and prolate shapes [14]. By analyzing nearly spherical vesicles with relative volumes v close to 1, stable nonaxisymmetric shapes have been shown by an approximate method to fill this gap [17]. These

nonaxisymmetric shapes are the intermediate states in the continuous transformation between oblate and prolate axisymmetric shapes.

A more general description of the bilayer structure takes into account that the two monolayers can undergo relative area changes at constant area of the neutral surface of the bilayer [8,18–20]. That means that, in contrast to the strict bilayer-couple model, ΔA may differ from the corresponding ΔA_0 defined for the unstressed monolayers. The energy contribution that results from this relative monolayer stretching (nonlocal bending energy) is comparable to the (local) bending energy of the membrane [21]. Accordingly, a proper description of the real vesicle structure is based on both energy contributions [8,22–24]. The theoretical concept that includes the nonlocal bending energy instead of the hard constraint of constant ΔA is called here the generalized bilayer-couple model. This model involves both the spontaneous-curvature as well as the strict bilayer-couple models as limiting cases. It has been shown that this general model provides an appropriate basis for the description of membrane tether experiments [21,22] as well as for the interpretation of the budding phenomenon of phospholipid vesicles [2,23–25]. A study of the transformation between prolate shapes and pear shapes on the basis of this model revealed that the nature of transitions between shapes of different classes is strongly influenced by the relative contribution of the nonlocal bending energy to the elastic energy of the bilayer membrane [26].

Most of the previous work on vesicle shapes has been based on mathematical methods which are restricted to axisymmetric shapes, and instead of a complete stability analysis, the shapes with the lowest membrane elastic energies were assumed to be stable. Such approaches leave open the questions (i) whether there are locally stable shapes of higher elastic energies, (ii) whether the axisymmetric shapes found are stable with respect to nonaxisymmetric deformations, and (iii) what the nonaxisymmetric shapes look like. As mentioned above, until now these questions have been answered only within the strict bilayer-couple model on the basis of an approximate method valid only for nearly spherical shapes [17].

The present paper is mainly aimed to provide a detailed study of that region of the phase diagram where oblate and prolate axisymmetric shapes transform into each other through nonaxisymmetric shapes. This study is based on the generalized bilayer-couple model. The calculations also include shapes of vesicles with low relative volumes. Furthermore, the stability of stationary shapes is analyzed. Particular emphasis is given to the character of the transition of oblate and prolate axisymmetric shapes into nonaxisymmetric shapes.

For this, a new variational method to calculate equilibrium shapes is developed. It is based on a Ritz procedure (see, e.g., [27]) expressing the shape function as a series of spherical harmonics. Keeping the values of the various quantities subjected to constraints constant, the membrane elastic energy is minimized with respect to amplitudes of spherical harmonics. This approach is general in the sense that it enables the calculation of both axisymmetric and nonaxisymmetric shapes as well as the stability analysis of stationary shapes with respect to all possible deformations. The stability analysis is based on the values of second derivatives of the elastic energy with respect to amplitudes of spherical harmonics. The only limitation of the present method is that the shapes must be representable by unique functions of the spherical angles.

This method is applied to shapes of simple phospholipid vesicles, assuming that their bilayer membrane is symmetric. In this case, the spontaneous curvatures of the two monolayers have the same absolute value but opposite signs. Thus the effect of the intrinsic curvature of the constituent lipids is negligible.

II. GENERALIZED BILAYER-COUPLE MODEL BY SPHERICAL HARMONICS

Equilibrium shapes of phospholipid vesicles are assumed to correspond to the minimum of the elastic energy of the closed bilayer membrane. The elastic energy is taken as the sum of the membrane bending energy W_b and the energy of relative monolayer stretching W_r (cf. [8,24,26,28]):

$$W = W_b + W_r = \frac{1}{2} k_c \int (C_1 + C_2)^2 dA + \frac{1}{2} \frac{k_r}{A_0} \left[\frac{\Delta A - \Delta A_0}{h} \right]^2 . \tag{1}$$

Here, k_c and k_r are the local and the nonlocal bending moduli, respectively, and C_1 and C_2 denote the two principal curvatures. Integration is performed over the neutral surface of the bilayer with the area A_0. The area difference between the outer and the inner leaflets of the phospholipid bilayer is denoted by ΔA. The corresponding spontaneous difference ΔA_0 is defined for the unstretched monolayers. The separation distance between the neutral surfaces of the two monolayers is denoted by h. The instantaneous value of the area difference ΔA is calculated as follows:

$$\Delta A = h \int (C_1 + C_2) dA . \tag{2}$$

For symmetric bilayers, which are considered here, k_r is related to the area expansivity modulus of the membrane k_t by the equation

$$k_r = h^2 \frac{k_t}{4} . \tag{3}$$

The minimization of the elastic energy [Eq. (1)] is performed at constant values of the membrane area A and the vesicle volume V. For given values of these quantities A_0 and V_0, respectively, the equilibrium shapes have to fulfill the constraints

$$A \equiv \int dA = A_0 , \tag{4}$$

$$V \equiv \int dV = V_0 . \tag{5}$$

A normalization of the elastic energy and the two con-

straints with respect to a sphere that has the surface area A_0 and the radius $R_s=(A_0/4\pi)^{1/2}$, and whose monolayers are unstretched, yields dimensionless model quantities w, w_b, w_r, Δa, a, and v, respectively. Due to this normalization, the elastic energy w is measured in units of the bending energy of the sphere ($8\pi k_c$). A dimensionless shape function $r=r(\vartheta,\varphi)$ is obtained by normalizing the original shape function with respect to R_s. Accordingly, the vesicle shape is described in terms of the distance r between the origin of the coordinate system and the closed surface of the vesicle using the spherical angles ϑ and φ as independent coordinates. It is required that r be a unique function of ϑ and φ. By the use of $r(\vartheta,\varphi)$, the elastic energy is expressed as

$$w=w_b+w_r$$
$$=\frac{1}{16\pi}\int\left[2r-\Delta r+\frac{r[\nabla r]^2+\frac{1}{2}\nabla r\cdot\nabla([\nabla r]^2)}{r^2+[\nabla r]^2}\right]^2 \times\frac{d\Omega}{r\sqrt{r^2+[\nabla r]^2}}+q(\Delta a-\Delta a_0)^2 , \quad (6)$$

where

$$\Delta a=\frac{1}{8\pi}\int\left[2r+\frac{r[\nabla r]^2+\frac{1}{2}\nabla r\cdot\nabla([\nabla r]^2)}{r^2+[\nabla r]^2}\right]d\Omega \quad (7)$$

and Δa_0 is defined as $\Delta a_0=\Delta A_0/8\pi hR_s$. The two constraints become

$$a\equiv\frac{1}{4\pi}\int r\sqrt{r^2+[\nabla r]^2}\,d\Omega=a_0\equiv 1 , \quad (8)$$

$$v\equiv\frac{1}{4\pi}\int r^3 d\Omega=v_0 . \quad (9)$$

Integration is performed over the full solid angle $d\Omega=\sin\vartheta\,d\vartheta\,d\varphi$. The differential operators ∇ and Δ, respectively, are applied to r as follows:

$$\nabla r=\left[r_\vartheta,\frac{1}{\sin\vartheta}r_\varphi\right] , \quad (10)$$

$$\Delta r=r_{\vartheta\vartheta}+\frac{\cos\vartheta}{\sin\vartheta}r_\vartheta+\frac{1}{\sin^2\vartheta}r_{\varphi\varphi} , \quad (11)$$

where r_t denotes the partial derivative of r with respect to t. The parameter q introduced in Eq. (6) is the ratio between the nonlocal and local bending moduli:

$$q=\frac{k_r}{k_c} . \quad (12)$$

In this way, v_0 and Δa_0 are obtained as basic geometric model parameters while q reflects the relative resistance of the membrane to monolayer stretching with regard to its resistance to bending.

In order to obtain extrema of Eq. (6), a Ritz procedure using spherical harmonics is applied. Accordingly, $r(\vartheta,\varphi)$ is expressed as a series of spherical harmonics $Y_{lm}(\vartheta,\varphi)$:

$$r(\vartheta,\varphi)=\sum_{l=0}^{\infty}\sum_{m=-l}^{l}u_{lm}Y_{lm}(\vartheta,\varphi) . \quad (13)$$

The functions $Y_{lm}(\vartheta,\varphi)$ are defined by the associated Legendre polynomials $P_{lm}(\cos\vartheta)$ as

$$Y_{lm}(\vartheta,\varphi)=\left[\frac{2l+1}{4\pi}\frac{(l-m)!}{(l+m)!}\right]^{1/2}P_{lm}(\cos\vartheta)e^{im\varphi} . \quad (14)$$

Since $r(\vartheta,\varphi)$ is a real function,

$$u_{l,-m}=(-1)^m u_{lm}^* . \quad (15)$$

The Ritz procedure used here requires the origin of the coordinate system to be fixed in an appropriate way. This yields six additional constraints for the calculation of equilibrium shapes. The necessity for the inclusion of such constraints, the present choice for the position of the coordinate system, and the resulting expressions are given in the Appendix.

Finally, for the calculation of equilibrium shapes the function

$$g=w+\lambda_a(a-1)+\lambda_v(v-v_0)+\lambda_x x_m+\lambda_y y_m+\lambda_z z_m +\lambda_{t_1}t_1+\lambda_{t_2}t_2+\lambda_{t_3}t_3 \quad (16)$$

must be minimized. It contains the membrane elastic energy and includes all eight constraints via Lagrange multipliers (λ). In the numerical computations, w, a, v, x_m, y_m, z_m, t_1, t_2, and t_3 are replaced by their definitions given above and in the Appendix. Since only a finite number of spherical harmonics can be used, the expansion (13) has to be cut at an appropriately chosen maximal l value $l_{\max}$.

A necessary condition to obtain equilibrium states is that the partial derivatives of g with respect to all amplitudes of spherical harmonics as well as to Lagrange multipliers vanish. Let us call a shape for which this condition is fulfilled a stationary shape. Accordingly, a stationary state is a solution of the system of nonlinear equations formed by the first derivatives of g. This equation system is solved numerically by the use of Newton's method where the values of integrals in Eqs. (6)–(9) and (A1)–(A3) (see the Appendix) as well as of integrals of the corresponding derivatives are obtained by a two-dimensional Simpson integration.

In order to decide whether a stationary shape obtained in this way minimizes the elastic energy, one has to perform a stability analysis of the corresponding solution. This is possible by using the same procedure as described in [17]. This procedure takes into account that the amplitudes of spherical harmonics are interrelated due to the presence of constraints. Its basic idea is to take some amplitudes to depend on the others and to inspect the eigenvalues of the matrix of second derivatives of the bending energy with respect to independent amplitudes. If these eigenvalues are all positive, the corresponding solution is stable, i.e., the stationary state characterizes a shape of minimum membrane elastic energy.

It should be noted that, strictly speaking, the present method to calculate stationary shapes as well as the stability analysis are valid only within the frame of the finite number of spherical harmonics used. However, if $l_{\max}$ is so large that its further increase would not change the re-

sults significantly, and if the number of integration intervals in the Simpson procedure is also correspondingly high, the present mathematical method will be sufficiently general and accurate.

III. NONAXISYMMETRIC SHAPES IN THE STRICT BILAYER-COUPLE MODEL ($q \to \infty$)

Let us first inspect the results of the calculations of equilibrium shapes for $q \to \infty$. This case is called the strict bilayer-couple model. It is identical with the assumption that not only the bilayer as a whole, but also both monolayers, have constant areas. In this special case of the present model, the nonlocal bending energy w_r vanishes. Instead of the corresponding energy contribution, a "hard" constraint requiring $\Delta a = \Delta a_0$ has to be included into the calculations. This strict bilayer-couple model has been extensively investigated [10–14,16], and for nearly spherical vesicles it has been used also for the calculation of nonaxisymmetric shapes [17]. It is interesting therefore to compare the previous results on nonaxisymmetric shapes obtained by a less accurate approach with the results of the method presented here, and additionally, to consider shapes that are not nearly spherical. On the other hand, the accuracy of the present method, which is still approximate, can be estimated for axisymmetric shapes by comparing the results with those of an Euler-Lagrange procedure (cf., e.g., [11,13,14]). The latter method is an exact method but has been applied only to axisymmetric shapes until now.

In the following, the computations are performed at the relative volumes $v_0 = 0.95$, $v_0 = 0.85$, and $v_0 = 0.7$. For the shape calculations at $v_0 = 0.95$ and $v_0 = 0.85$, the expansion of the shape function in spherical harmonics

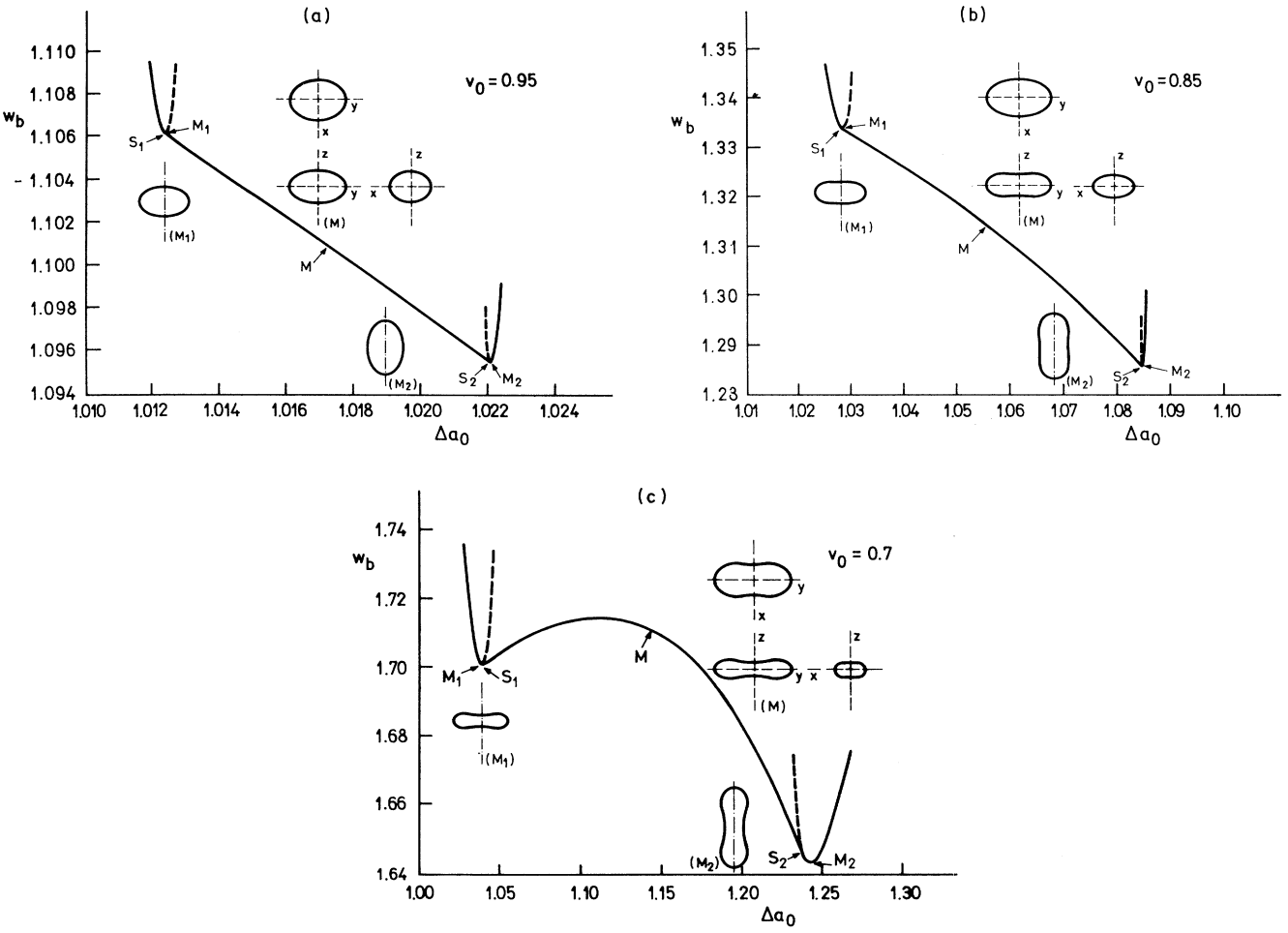

FIG. 1. Relative bending energies w_b of stationary shapes as functions of relative differences Δa_0 of monolayer areas for $q \to \infty$ at the relative volumes (a) $v_0 = 0.95$, (b) $v_0 = 0.85$, and (c) $v_0 = 0.7$. Dashed lines mark unstable shapes. S_1, S_2: symmetry-breaking points where axisymmetric oblate shapes and axisymmetric prolate shapes, respectively, transform into nonaxisymmetric shapes. M_1, M_2: minimum points of the curves belonging to the two classes of axisymmetric shapes. M: intermediate points of the nonaxisymmetric shape class. Shapes corresponding to the points given in parentheses are included. The axisymmetric shapes belonging to M_1 and M_2 are marked by including their symmetry axes as vertical lines. The nonaxisymmetric shapes (M) are represented by three cuts containing the reflection planes where every reflection plane contains a pair of axes of the Cartesian coordinate system.

[Eq. (13)] is cut at $l_{max}=10$. At $v_0=0.7$, the value $l_{max}=22$ is used. For the shapes studied in the present paper, these l_{max} values provide a sufficiently high accuracy of the Ritz method (see below). For even lower volumes, the application of the present method meets with difficulties since the corresponding shapes cannot be represented by unique functions of the spherical angles.

Figures 1(a)–1(c) present the results of the calculations of nonaxisymmetric shapes as well as of those axisymmetric shapes which are obtained in the same ranges of the model parameters. The relative bending energy of stationary shapes is shown for the three relative volumes as a function of Δa_0. Here, and also in the following, only those axisymmetric shapes are included that can be directly transformed into nonaxisymmetric shapes through the symmetry-breaking points S_1 and S_2 by changing Δa_0. The two axisymmetric shape classes comprise shapes that are mirror symmetric with respect to their equatorial planes. These shapes are oblate at low Δa_0 values and prolate at high Δa_0 values. The points M_1 and M_2 designate the minima of the bending energy w_b with respect to Δa_0 for each of the two classes. The contours of the shapes corresponding to these points are shown in Figs. 1(a)–1(c).

All nonaxisymmetric shapes obtained by the present method at the chosen relative volumes are characterized by three orthogonal reflection planes. Accordingly, they can be visualized by the contours of those three cuts that contain the symmetry planes. One example is shown for every relative volume in Figs. 1(a)–1(c). Neighboring shapes of different classes transform smoothly into each other through the symmetry-breaking points S_1 and S_2. Therefore the nonaxisymmetric shapes provide a continuous pathway from oblate to prolate axisymmetric shapes at increasing Δa_0. Example shapes obtained during such a transformation are shown for $v_0=0.7$ in Fig. 2, where a nonaxisymmetric shape (b) represents an intermediate state between a discocyte (a) and a dumbbell (c,d). In order to illustrate how shape (b) transforms into the dumbbell (d), this dumbbell is shown also in that orientation in which it is obtained from shape (b) by a continuous increase of Δa_0.

The stability analysis has been performed at $v_0=0.95$ and $v_0=0.85$. The shapes corresponding to the dashed-line branches in Figs. 1(a) and 1(b) have been found to be unstable. (These shapes are characterized by saddle points in the energy "surface.") Because of the full analogy of the results of calculations of stationary shapes at different relative volumes it is assumed that the stability behavior is the same for $v_0=0.7$ as for the two higher volumes. The corresponding curves of unstable shapes in Fig. 1(c) are also drawn as dashed lines. The locally stable shapes denoted by solid lines have the lowest bending energies at given Δa_0 values, i.e., they are also globally stable.

In order to estimate the accuracy of the present Ritz method, the bending energies of axisymmetric shapes belonging to the points M_1 and M_2 were recalculated using various l_{max} values. The results were compared with corresponding results of the Euler-Lagrange procedure men-

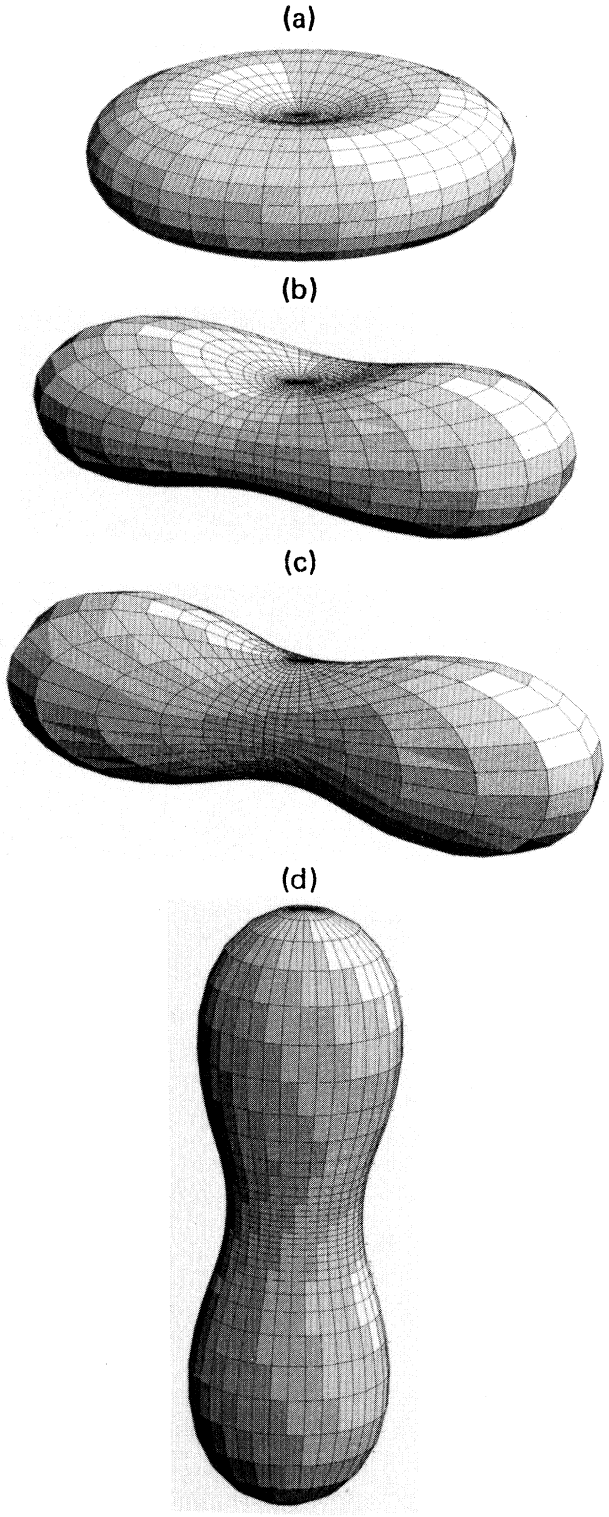

FIG. 2. Examples of stationary vesicle shapes obtained at $v_0=0.7$. Shapes (a), (c), and (d) are axisymmetric, where (c) and (d) represent the same dumbbell shape in different orientations with respect to the fixed reference frame. The two shapes (a) and (c,d) belong to the points M_1 and M_2, respectively [see Fig. 1(c)]. Shape (b) is a nonaxisymmetric intermediate shape between (a) and (c) corresponding to point M in Fig. 1(c).

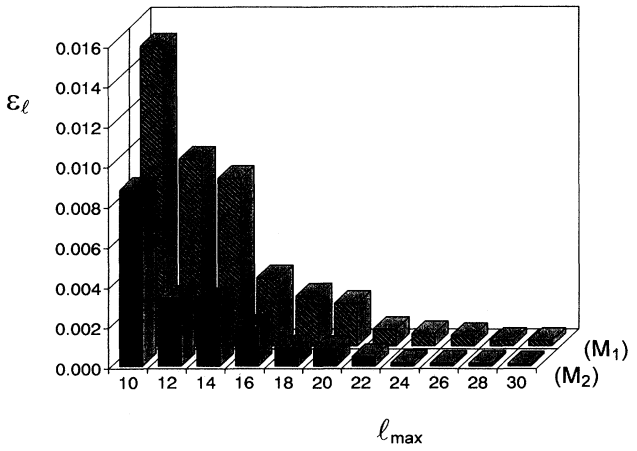

FIG. 3. Relative differences ε_l between the bending energies $w_b(l_{max})$ calculated by the present method and the corresponding values w_{EL} obtained by an Euler-Lagrange procedure in dependence on l_{max}: $\varepsilon_l=[w_b(l_{max})-w_{EL}]/w_{EL}$. The values of ε_l were obtained for $v_0=0.7$ at the points M_1 and M_2, respectively [cf. Fig. 1(c)].

tioned above. Figure 3 shows the relative differences of related bending energies obtained by the two methods at $v_0=0.7$ as functions of l_{max}. For $l_{max}=22$, these relative differences are smaller than 10^{-3}. Therefore this l_{max} value is used in the shape calculations at $v_0=0.7$. The accuracy of the Ritz method at M_1 and M_2 is even higher at the relative volumes 0.85 and 0.95, where $l_{max}=10$ is used. (The error is of the order 10^{-4} for $v_0=0.85$ and smaller than 10^{-6} for $v_0=0.95$.) Because the nonaxisymmetric shapes are characterized by Δa_0 values between those of M_1 and M_2, it can be assumed that they are also calculated with sufficiently high accuracy. Finally, it should be noted that the present results obtained at $v_0=0.95$ confirm the previous approximate results [17].

IV. GENERALIZED BILAYER-COUPLE MODEL

A. General remarks

In the following, the effect of a finite value of q on the calculations of vesicle shapes is studied. In this case, the two monolayers are assumed to undergo relative area stretching, i.e., Δa is in general different from Δa_0. Then an equilibrium shape is characterized by that Δa value which minimizes the elastic energy w [Eq. (6)] at constant values of the relative membrane area [$a=1$, Eq. (8)] and the relative volume [$v=v_0$, Eq. (9)]. Accordingly, at equilibrium it is required that

$$\frac{\partial g}{\partial \Delta a}=0 , \tag{17}$$

with g defined in Eq. (16). Thus the condition

$$\left.\frac{\partial w}{\partial \Delta a}\right|_{eq}=0$$

is obtained, which yields the useful relation

$$\left.\frac{\partial w_b}{\partial \Delta a}\right|_{eq}=-2q(\Delta a-\Delta a_0) . \tag{18}$$

The left-hand side of Eq. (18) depends neither on q nor on Δa_0. Therefore it is the same for a given stationary shape characterized by a certain Δa value at any value of q. The right-hand side of Eq. (18) determines for a given q the Δa_0 value of this stationary shape, i.e., its location in the phase diagram. Thus a shape that is stationary for $q\to\infty$ is also stationary at finite q, and the values of the left-hand side of Eq. (18) obtained within the strict bilayer-couple model can be taken as the basis for corresponding calculations in the generalized bilayer-couple model.

Furthermore, some information about the stability properties of stationary shapes obtained for $q\to\infty$ can be applied to the case of finite q values. A stationary shape that is unstable for $q\to\infty$ is unstable with respect to some shape changes that conserve Δa. For finite q also shape changes that do not conserve Δa are allowed, but the stationary shape remains unstable with respect to the same Δa-conserving shape changes as for $q\to\infty$. Thus shapes that are unstable for $q\to\infty$ cannot be stable for finite values of q. On the other hand, as will be shown in the further discussion, the proof that a shape is stable at $q\to\infty$ is not sufficient to conclude that it is also stable at finite q.

These properties are used to visualize [based on Eq. (18)] the behavior of the system representing the generalized bilayer couple model in a general way (cf. [26]). Let us consider both sides of Eq. (18) as functions of Δa. Then, the stationary states fulfilling this equation are obtained at the intersections of the graphs of these two functions. The graphs of

$$\left.\frac{\partial w_b}{\partial \Delta a}\right|_{eq}$$

as functions of Δa are depicted for the relative volumes 0.85 and 0.7 in Figs. 4(a) and 4(b), respectively. It is important to note that none of the lines shown are strictly vertical, although some are very steep. (Points on the solid line to the left and below S_1, and to the right and above S_2, correspond to axisymmetric shapes, and points on the line between S_1 and S_2 correspond to nonaxisymmetric shapes.) Dashed-line branches correspond to those stationary shapes that were found to be unstable for $q\to\infty$ (see Sec. III). The graphs of the right-hand side of Eq. (18) as functions of Δa are straight lines. The slope of such a straight line is given by $-2q$, and Δa_0 determines the crossing of this line with the axis of the abscissa. Thus the case $q\to\infty$ can be represented by vertical lines. As will be discussed below, a characteristic value for phospholipid bilayers is $q=3$. Some examples of straight lines obtained for $q=3$ at different Δa_0 values are included in Figs. 4(a) and 4(b) (dotted lines). The various crossing points between the graphs of the two sides of Eq. (18) as obtained from subsequent parallel shifts of a straight line denote the possible transformations of a stationary shape with respect to variations of Δa_0.

The straight vertical lines corresponding to $q\to\infty$ (not

shown) move at increasing values of $\Delta a_0 = \Delta a$ from the left to the right in Figs. 4(a) and 4(b). All vertical lines cross the stable branches of the graphs of

$$\left.\frac{\partial w_b}{\partial \Delta a}\right|_{\text{eq}}$$

only once. This is the expected result, which shows that for $q \to \infty$ the transition between oblate and prolate axisymmetric shapes through nonaxisymmetric shapes is continuous.

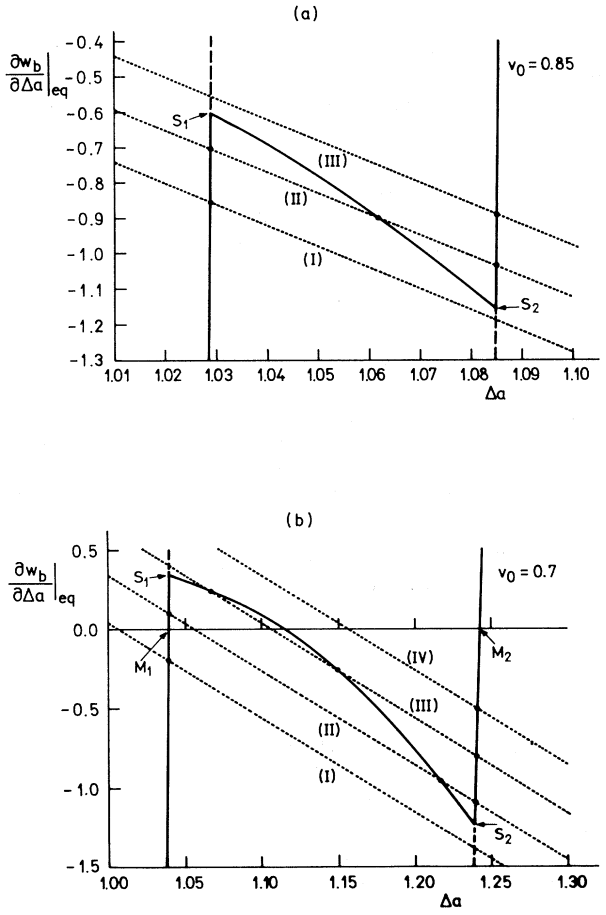

FIG. 4. Graphical solution of Eq. (18). The Δa dependencies of $\partial w_b/\partial \Delta a$ at equilibrium are shown for the relative volumes (a) $v_0 = 0.85$ and (b) $v_0 = 0.7$. These dependencies, which are the same for any value of q, were calculated within the strict bilayer-couple model. Note that some lines are very steep but not vertical. The results of the stability analysis at $q \to \infty$ are included by drawing the lines belonging to stable shapes solid and those corresponding to unstable shapes dashed. Examples of straight lines representing graphs of the right-hand side of Eq. (18) for $q = 3$ are included (dotted lines). They are marked by roman numbers and their order corresponds to increasing values of Δa_0. In (b) the corresponding Δa_0 values are given at the crossings of lines (I)–(IV) with the axis of the abscissa. Crossings of solid and dotted lines are marked by points (see text). For other notations see Fig. 1.

B. Finite values of q

A characteristic value for phospholipid bilayers is $q = 3$. For example, the ratio between the nonlocal and local bending moduli can be obtained from the values $k_c = 1.2 \times 10^{-19}$ J and $k_r = 4.1 \times 10^{-19}$ J [21]. For these values $q = 3.4$. Another estimation can be made by using Eq. (3) and taking the area expansivity modulus of the bilayer as $k_t = 0.2\ \text{J m}^{-2}$ [29]. The distance h between the two monolayers is measured between their neutral surfaces. Accordingly, it is approximately half of the membrane thickness. Assuming $h = 2.7 \times 10^{-9}$ m, Eq. (3) yields $k_r = 3.65 \times 10^{-19}$ J, which also gives $q \approx 3$. In the following part of this section, the generalized bilayer-couple model is first studied for $q = 3$. Subsequently, the results are generalized for arbitrary values of q.

For $q = 3$, the behavior of the system differs significantly from the results of the strict bilayer-couple model. It is also different for different relative volumes. Let us inspect the various stationary states obtained at the intersections of dotted and solid lines in Fig. 4(a) ($v_0 = 0.85$) and 4(b) ($v_0 = 0.7$). Corresponding to different ranges of Δa_0 values, three different situations can be distinguished in the appearance of stationary shapes:

(i) There is only one stationary shape at the given Δa_0. In this case, the straight dotted line crosses the stables branches of the graphs of the left-hand side of Eq. (18) only once. The stationary states designated by such single intersections correspond to stable oblate shapes [lines (I) in both Figs. 4(a) and 4(b)] or to stable prolate shapes [line (III) in Fig. 4(a) and line (IV) in Fig. 4(b)].

(ii) There are three crossings between a straight dotted line and the various solid lines, and the solid line connecting S_1 and S_2 and characterizing nonaxisymmetric shapes is crossed only once [lines (II) in both Figs. 4(a) and 4(b)]. In this case the outer two crossing points belong to axisymmetric shapes and denote locally stable stationary states whereas the intermediate intersection marks an unstable nonaxisymmetric shape. The elastic energy of the latter shape has a *maximum* with respect to varying Δa values at constant Δa_0.

(iii) The dotted line crosses the solid lines again three times, but now two of the crossing points belong to nonaxisymmetric shapes [line (III) in Fig. 4(b)]. Again, the intermediate crossing point denotes an unstable stationary state while the outer two crossings characterize locally stable shapes.

In this way, for $q = 3$ all nonaxisymmetric shapes at $v_0 = 0.85$ are found to be unstable [cf. Fig. 4(a)]. At $v_0 = 0.7$ there are, depending on the value of Δa_0, either only unstable or coexisting unstable and locally stable stationary nonaxisymmetric shapes [cf. Fig. 4(b)]. In order to establish the globally stable shapes as well as the possible shape transformations at variations of Δa_0, the elastic energies of different stationary states have to be compared. These elastic energies (for $q = 3$) are shown as functions of Δa_0 in Fig. 5 ($v_0 = 0.85$) and Fig. 6 ($v_0 = 0.7$). The critical regions of the two figures contain the symmetry-breaking points S_1 and S_2. These regions are enclosed in boxes in part (a) of each figure and enlarged

in Figs. 5(b) and 6(b). Dashed lines again denote unstable, i.e., nonexisting, shapes. As mentioned above, at a given Δa_0 between S_1 and S_2 there are three stationary states, two corresponding to locally stable shapes (solid lines) and one corresponding to an unstable shape (dashed line). The shape that belongs to the solid line with the lowest elastic energy is globally stable. It is seen that the locally stable nonaxisymmetric shapes at $v_0=0.7$ are metastable, i.e., they also do not exist. The vertically measured distance between the dashed line and the closest solid line denotes in both Figs. 5 and 6 the height of the energy barrier that has to be overcome during a transformation of shapes of the two locally stable classes into each other at a given Δa_0. This energy barrier is largest at the point P_T, where oblate and prolate shapes have the same energy. At this point, its value is in both cases smaller than $10k_BT$. Accordingly, for every Δa_0 value the vesicle will quickly assume the shape of the lowest elastic energy. Thus the transition of oblate and prolate axisymmetric shapes into each other at variations of Δa_0 is direct and discontinuous and is expected at that Δa_0 value where the shapes of both classes have the same energy (point P_T).

The analogous calculations were also performed at $v_0=0.95$. The corresponding results are qualitatively the same as at $v_0=0.85$ and are not shown separately.

It has been shown in this way that there are no globally stable nonaxisymmetric shapes for $v_0\geq 0.7$ and $q=3$. However, it is worthwhile to note that the experimentally measured q values are spread over a broad range. Moreover, they depend on the composition of the bilayer. It is of interest therefore to study the generalized bilayer-couple model for a broader range of q values. It can be

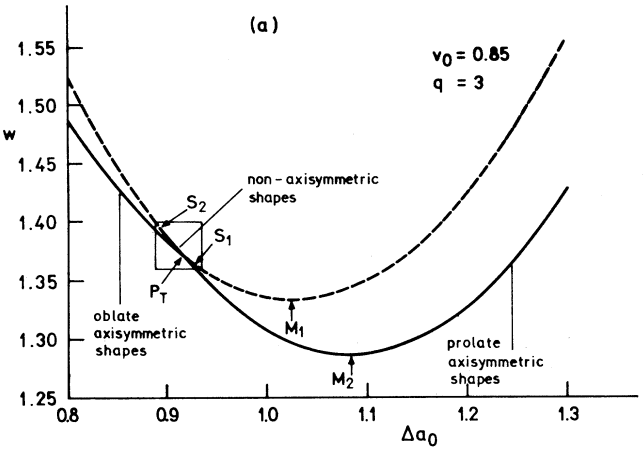

FIG. 5. Relative elastic energies w of stationary shapes as functions of Δa_0 for $q=3$ at the relative volume $v_0=0.85$. (b) enlarges the region marked by the frame in (a). Dashed lines denote unstable shapes. P_T: point of the discontinuous transition between oblate and prolate shapes. For other notations see Fig. 1.

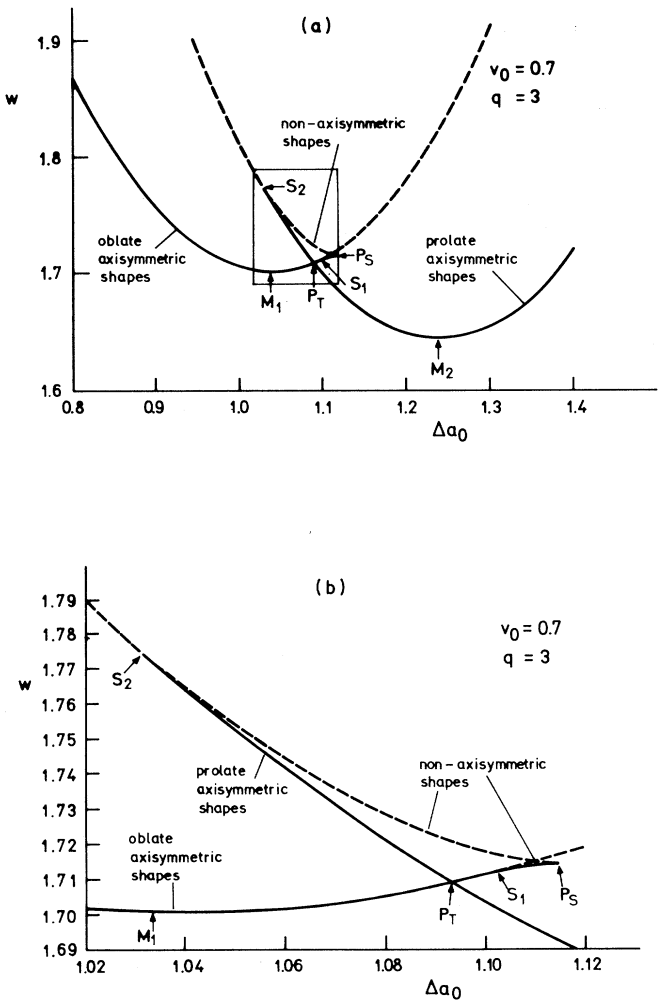

FIG. 6. The analogous graphs as shown in Fig. 5 are presented for the relative volume $v_0=0.7$ ($q=3$). P_S: point where the stable branch and the unstable branch of the $w(\Delta a_0)$ dependence of stationary nonaxisymmetric shapes merge. For other notations see Fig. 5.

seen from Figs. 4(a) and 4(b) that the system exhibits a high sensitivity with respect to variations of q, i.e., to variations of the slope of the straight lines corresponding to the right-hand side of Eq. (18).

The influence of q on the calculations of vesicle shapes is studied in more detail at the relative volume $v_0=0.7$. The ranges of values of Δa_0 and q at which locally stable shapes of different classes exist are mapped in "phase-diagram" form in Fig. 7. A vertical cut through this phase diagram at $q=3$ is given by Fig. 6, where the corresponding dependence of the elastic energy w on Δa_0 is depicted. Another analogous cut that would be obtained for $q\rightarrow\infty$ is represented by Fig. 1(c). The curves in Fig. 7 labeled s_1, s_2, p_S, and p_T correspond to the points so labeled (capital letters) in Fig. 6, for example. The crossing points of different lines are denoted by T_1, T_2, T_3, and T_4.

Let us first consider the globally stable shapes of the three different classes. The regions in which these shapes exist in the q-Δa_0 phase diagram (Fig. 7) are delineated by solid lines. The transitions between globally stable shapes of different classes for changing Δa_0 are continuous as long as the solid lines are symmetry-breaking lines (s_1 or s_2). Thus globally stable nonaxisymmetric shapes and globally stable oblate shapes transform into each other continuously through the s_1 line at q values that are greater than the q value of T_2. The corresponding transition between nonaxisymmetric shapes and prolate shapes (s_2 line) is continuous only for q values greater than q corresponding to T_4. At these q values, the symmetry-breaking lines s_1 and s_2 divide the phase diagram into three regions where all locally stable shapes are also globally stable. This situation is qualitatively the same as in the strict bilayer-couple model [cf. Fig. 1(c)]. For q values between those of T_2 and T_4, the transition between globally stable nonaxisymmetric shapes and globally stable prolate shapes is discontinuous and takes place at the p_T line. At q values lower than q corresponding to T_2, all globally stable shapes are axisymmetric, and the p_T line denotes the discontinuous transition between oblate and prolate shapes (cf. Fig. 6). It is worthwhile to note that the value $q=3$ is only slightly smaller than the q value corresponding to T_2 (see also Table I). Accordingly, a small increase of q with respect to $q=3$ is already sufficient to obtain globally stable nonaxisymmetric shapes at $v_0=0.7$.

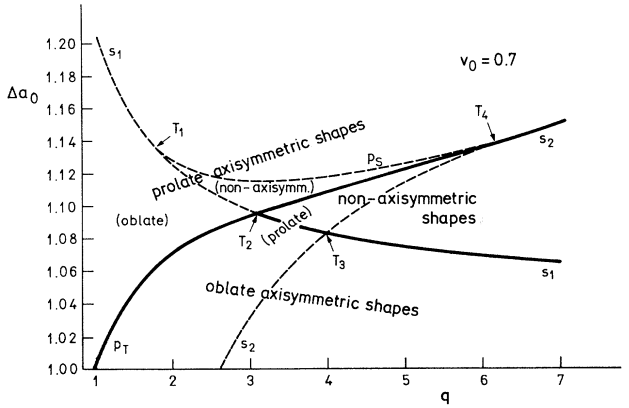

FIG. 7. Phase diagram presenting the Δa_0 regions of locally stable shapes in dependence on q at $v_0=0.7$. s_1,s_2,p_S,p_T: separation lines of different regions of locally stable shapes. The notation of these lines (lowercase letters) corresponds to the notation of points [uppercase letters, see Figs. 1(c) and 6], which generate these lines at variations of q. Solid lines separate the three regions of globally stable shapes. Dashed lines subdivide these regions by marking the regions of metastable shapes (identified in parentheses). T_1,T_2,T_3,T_4: crossing points of different separation lines.

TABLE I. The coordinates of characteristic points in the q-Δa_0 phase diagram of locally stable shapes are listed for different relative volumes. T_1, T_2, T_3, and T_4 correspond to the crossings of various separation lines in this phase diagram and are defined in Fig. 7.

	$v_0=0.7$		$v_0=0.85$		$v_0=0.95$	
	q	Δa_0	q	Δa_0	q	Δa_0
T_1	1.810	1.136	4.169	0.958	5.306	0.914
T_2	3.118	1.096	4.700	0.966	5.368	0.915
T_3	4.000	1.083	4.988	0.969	5.449	0.917
T_4	6.260	1.139	5.883	0.987	5.610	0.920

The dashed lines in Fig. 7 denote the regions of metastable shapes, i.e., of locally stable shapes with higher elastic energies than the coexisting globally stable shapes. The classes containing the corresponding metastable shapes are identified in parentheses. As mentioned above, there is only a small energy barrier between coexisting metastable and globally stable shapes. Therefore the metastable shapes are not expected to exist.

The values of q and Δa_0 belonging to the crossing points T_1, T_2, T_3, and T_4 of different separation lines (cf. Fig. 7) as well as the corresponding values obtained for the related points at $v_0=0.85$ and $v_0=0.95$ are listed in Table I. At increasing v_0 the analogous regions of locally stable shapes become smaller in comparison with Fig. 7 (cf. Table I). The general behavior at the higher relative volumes is qualitatively the same as for $v_0=0.7$ with the following exception. The sign of the ordinate of S_1 in the graphs of Fig. 4 determines whether the s_1 line in Fig. 7 corresponds to positive or negative Δa_0 values for $q\rightarrow 0$. In contrast to the situation shown in Fig. 7, this line will be characterized by negative values of Δa_0 if the analogous calculations are performed for $q\rightarrow 0$ at $v_0=0.85$ [cf. Fig. 4(a)] and $v_0=0.95$. Accordingly, the subregion of metastable oblate shapes within the region of globally stable prolate shapes becomes much smaller at increasing relative volumes.

V. DISCUSSION AND CONCLUSIONS

The mathematical method to calculate vesicle shapes developed in this paper involves all shapes and their possible deformations which are representable by unique functions of the spherical angles. By increasing the num-

ber of spherical harmonics in the expansion of the shape functions, a sufficiently high accuracy of the calculations can be obtained for relative volumes not too small. This method is particularly useful for the study of nonaxisymmetric shapes which were only partly investigated until now. It also represents the basis for a general approach to simulate thermal fluctuations of vesicle shapes [30]. It should be noted, however, that the range of relative volumes considered here ($v_0 \geq 0.7$) cannot be extended to lower values because the shapes of vesicles with correspondingly small v_0 cannot be calculated by the present Ritz method. Thus the behavior of the system at smaller relative volumes may be different from the present results and remains an open problem.

The nonaxisymmetric stationary shapes obtained by the present numerical analysis involve three orthogonal reflection planes. Within the strict bilayer-couple model ($q \rightarrow \infty$), all stationary nonaxisymmetric shapes are globally stable, and they represent the intermediate states in the continuous transformation between oblate and prolate axisymmetric shapes. This is in agreement with previous findings [17].

Considering finite values of the ratio q between the nonlocal and the local elastic bending moduli, it has been shown that the behavior of the system, in particular the stability of stationary shapes and the character of shape transformations, are highly dependent on q. It is interesting that the range of q values corresponding to a discontinuous transition of oblate and prolate shapes into each other coincides with the experimentally measured q range. The present analysis shows that vesicles with relative volumes $v_0 \geq 0.7$ will not assume nonaxisymmetric shapes if $q = 3$, which is a characteristic value for phospholipid bilayers. This is in agreement with the fact that hitherto no observations of corresponding nonaxisymmetric shapes of phospholipid vesicles have been reported. It should be noted, however, that experimental reports of nonaxisymmetric shapes that could be related to the present work are in general lacking. On the other hand, axisymmetric shapes such as discocytes or dumbbells [cf. Figs. 2(a), 2(c), and 2(d)], which are stable in the present analysis, have often been observed [1–3,12]. Furthermore, it has been shown that vesicles can undergo reversible oblate-prolate shape transformations [31]. A more detailed experimental study of such transformations would be useful in order to illuminate this topic and could also yield a rough estimation of the parameter q. Possible experiments would require controlled changes of the relative volume v_0 of the vesicle as well as of the spontaneous area difference of monolayers Δa_0. The vesicle volume could be varied, e.g., by changing the osmolarity of the solution in which the vesicles are suspended. Varying the temperature causes changes of the membrane area of the vesicles, which is also reflected in changes of the *relative* volume v_0. Furthermore, in Refs. [2,12,31] the interpretation of the observed shape transformations has been based on assuming temperature-dependent variations of Δa_0. In general, a change of Δa_0 can be accomplished either by a change of the spontaneous area per molecule in one monolayer with respect to the other, or by varying the difference between the numbers of molecules of the two layers. This is possible by changing the chemical properties of the environment of a vesicle (see, e.g., [3]).

In any case, a large variability of the behavior of vesicles in related experiments can be expected due to the sensitivity of the system to small changes of q. At q values greater than a certain critical value depending on the relative volume, nonaxisymmetric shapes are stable (cf. Fig. 7 and Table I). In general, the value of q will rise if the number of bilayers forming a vesicle increases (cf. [28]), and q is certainly different for bilayers with different lipid compositions. Thus nonaxisymmetric shapes could be important, for example, in the study of multilamellar phospholipid vesicles as well as of closed bilayers composed of different lipid mixtures. The observation of ellipsoidal nonaxisymmetric shapes similar to the one shown in Fig. 2(b) has been reported for red blood cells [32]. Although the erythrocyte membrane has a more complex structure than pure phospholipid membranes, the existence of these elliptocytes might be related to a difference between the effective q values corresponding to the membranes of these cells and of normal red blood cells (axisymmetric discocytes).

ACKNOWLEDGMENTS

We would like to thank R. E. Waugh for his critical reading of the manuscript. This work has been supported by the German Academic Exchange Service for V.H. and by Grants Nos. P3-0244-381 and P1-0108-106 of The Ministry of Science and Technology of the Republic of Slovenia.

APPENDIX: FIXATION OF THE COORDINATE SYSTEM

According to Eq. (13), a given shape is represented by a set of amplitudes of spherical harmonics. However, different positions of the coordinate system obtained by translation and/or rotation yield different sets of amplitudes for the same shape. If the series of spherical harmonics were infinite, the elastic energy would be the same for all such different sets of amplitudes, i.e., the system would be degenerate. On the other hand, if a finite number of spherical harmonics is used, a change of the position of the reference frame by translation or rotation will slightly change the elastic energy. This artificial dependence of the energy on the position of the coordinate system is different for different shapes and also for different numbers of spherical harmonics included. Therefore it is necessary to fix the coordinate system in all computations in a uniform way. This is done here by introducing the following additional requirements (cf. [17]).

(i) The mass center of the vesicle is the origin of the coordinate system.

(ii) The z axis ($\vartheta = 0$) of the Cartesian coordinate system points into one of those directions for which the distance between the vesicle surface and the origin of the reference frame [$r(\vartheta,\varphi)$] has an extremum.

(iii) The x axis ($\vartheta = \pi/2$, $\varphi = 0$) is chosen in such a way that $r(\pi/2,\varphi)$ has an extremum with respect to rotations about the z axis.

The first requirement yields three constraints for the normalized coordinates x_m, y_m, and z_m of the mass center of the vesicle:

$$x_m \equiv \frac{3}{16\pi v_0}\int r^4 \sin\vartheta \cos\varphi \, d\Omega = 0 \ , \tag{A1}$$

$$y_m \equiv \frac{3}{16\pi v_0}\int r^4 \sin\vartheta \sin\varphi \, d\Omega = 0 \ , \tag{A2}$$

$$z_m \equiv \frac{3}{16\pi v_0}\int r^4 \cos\vartheta \, d\Omega = 0 \ . \tag{A3}$$

The second and third requirements, respectively, yield the conditions

$$\left.\frac{\partial r(\vartheta,\varphi)}{\partial \vartheta}\right|_{\vartheta=0} = 0 \ , \tag{A4}$$

$$\left.\frac{\partial r(\vartheta,\varphi)}{\partial \varphi}\right|_{\vartheta=\frac{\pi}{2},\varphi=0} = 0 \ . \tag{A5}$$

Using Eqs. (13)–(15), the condition (A4) is rewritten in terms of amplitudes of spherical harmonics as

$$-\frac{1}{2}\sum_{l=1}^{\infty}\left[\frac{2l+1}{4\pi}l(l+1)\right]^{1/2}[\cos\varphi(u_{l1}+u_{l1}^*)+i\sin\varphi(u_{l1}-u_{l1}^*)]=0 \ , \tag{A6}$$

where i is the imaginary unit and u_{l1}^* denotes the complex conjugate of u_{l1}. Since Eq. (A6) must be valid for any value of φ, two constraints are obtained from condition (A4):

$$t_1 \equiv \sum_{l=1}^{\infty}\left[\frac{2l+1}{4\pi}l(l+1)\right]^{1/2}(u_{l1}+u_{l1}^*)=0 \tag{A7}$$

and

$$t_2 \equiv \sum_{l=1}^{\infty}\left[\frac{2l+1}{4\pi}l(l+1)\right]^{1/2}(u_{l1}-u_{l1}^*)=0 \ . \tag{A8}$$

Finally, condition (A5) yields the constraint

$$t_3 \equiv \sum_{l=1}^{\infty}\sum_{m=1}^{l} m\left[\frac{2l+1}{4\pi}\frac{(l-m)!}{(l+m)!}\right]^{1/2}P_{lm}(0)(u_{lm}-u_{lm}^*)=0 \ . \tag{A9}$$

*Present address: Department of Biophysics, University of Rochester, 601 Elmwood Avenue, Rochester, New York 14642.

†FAX: (61) 311 540. Electronic address: Bostjan.Zeks@IJS.SI

[1] R. Lipowsky, Nature **349**, 475 (1991).
[2] J. Käs and E. Sackmann, Biophys. J **60**, 825 (1991).
[3] E. Farge and P. F. Devaux, Biophys. J. **61**, 347 (1992).
[4] *The Structure and Conformation of Amphiphilic Membranes,* edited by R. Lipowsky, D. Richter, and K. Kremer, Springer Proceedings in Physics Vol. 66 (Springer, Berlin, 1992).
[5] W. Helfrich, Z. Naturforsch. Teil C **28**, 693 (1973).
[6] H. J. Deuling and W. Helfrich, J. Phys. (Paris) **37**, 1335 (1976).
[7] H. J. Deuling and W. Helfrich, Biophys. J. **16**, 861 (1976).
[8] E. Evans, Biophys. J. **30**, 265 (1980).
[9] L. Miao, B. Fourcade, M. Rao, M. Wortis, and R. K. P. Zia, Phys. Rev. A **43**, 6843 (1991).
[10] S. Svetina and B. Žekš, Biomed. Biochim. Acta **44**, 979 (1985).
[11] S. Svetina and B. Žekš, Eur. Biophys. J. **17**, 101 (1989).
[12] K. Berndl, J. Käs, R. Lipowsky, E. Sackmann, and U. Seifert, Europhys. Lett. **13**, 659 (1990).
[13] S. Svetina and B. Žekš, J. Theor. Biol. **146**, 115 (1990).
[14] U. Seifert, K. Berndl, and R. Lipowsky, Phys. Rev. A **44**, 1182 (1991).
[15] M. P. Sheetz and S. J. Singer, Proc. Natl. Acad. Sci. USA **71**, 4457 (1974).
[16] S. Svetina, V. Kralj-Iglič, and B. Žekš, in *Proceedings of the Tenth School on Biophysics of Membrane Transport,* edited by J. Kuczera and S. Przestalski (Agricultural University of Wrocław, Wrocław, 1990), Vol. II, pp. 139–155.
[17] V. Heinrich, M. Brumen, R. Heinrich, S. Svetina, and B. Žekš, J. Phys. (France) II **2**, 1081 (1992).
[18] W. Helfrich, Z. Naturforsch. Teil C **29**, 510 (1974).
[19] E. Evans, Biophys. J. **14**, 923 (1974).
[20] S. Svetina, M. Brumen, and B. Žekš, Stud. Biophys. **110**, 177 (1985).
[21] R. E. Waugh, J. Song, S. Svetina, and B. Žekš, Biophys. J. **61**, 974 (1992).
[22] B. Božič, S. Svetina, B. Žekš, and R. E. Waugh, Biophys. J. **61**, 963 (1992).
[23] W. Wiese, W. Harbich, and W. Helfrich, J. Phys. Condens. Matter **4**, 1647 (1992).
[24] U. Seifert, L. Miao, H.-G. Döbereiner, and M. Wortis, in *The Structure and Conformation of Amphiphilic Membranes* (Ref. [4]), p. 93.
[25] J. Käs, E. Sackmann, R. Podgornik, S. Svetina, and B. Žekš, J. Phys. (France) II **3**, 631 (1993).
[26] S. Svetina and B. Žekš, in *Proceedings of the Eleventh School on Biophysics of Membrane Transport,* edited by J. Kuczera and S. Przestalski (Agricultural University of Wrocław, Wrocław, 1992), Vol. II, pp. 115–140.

[27] R. Courant and D. Hilbert, *Methoden der Mathematischen Physik* (Springer, Berlin, 1924).
[28] S. Svetina and B. Žekš, Eur. Biophys. J. **21**, 251 (1992).
[29] E. Evans and D. Needham, J. Phys. Chem. **91**, 4219 (1987).
[30] V. Heinrich, F. Sevšek, S. Svetina, and B. Žekš (unpublished).
[31] E. Sackmann, H. P. Duwe, and H. Engelhardt, J. Chem. Soc. Faraday Discuss. **81**, 281 (1986).
[32] J. Palek, Clin. Haematol. **14**, 45 (1985).

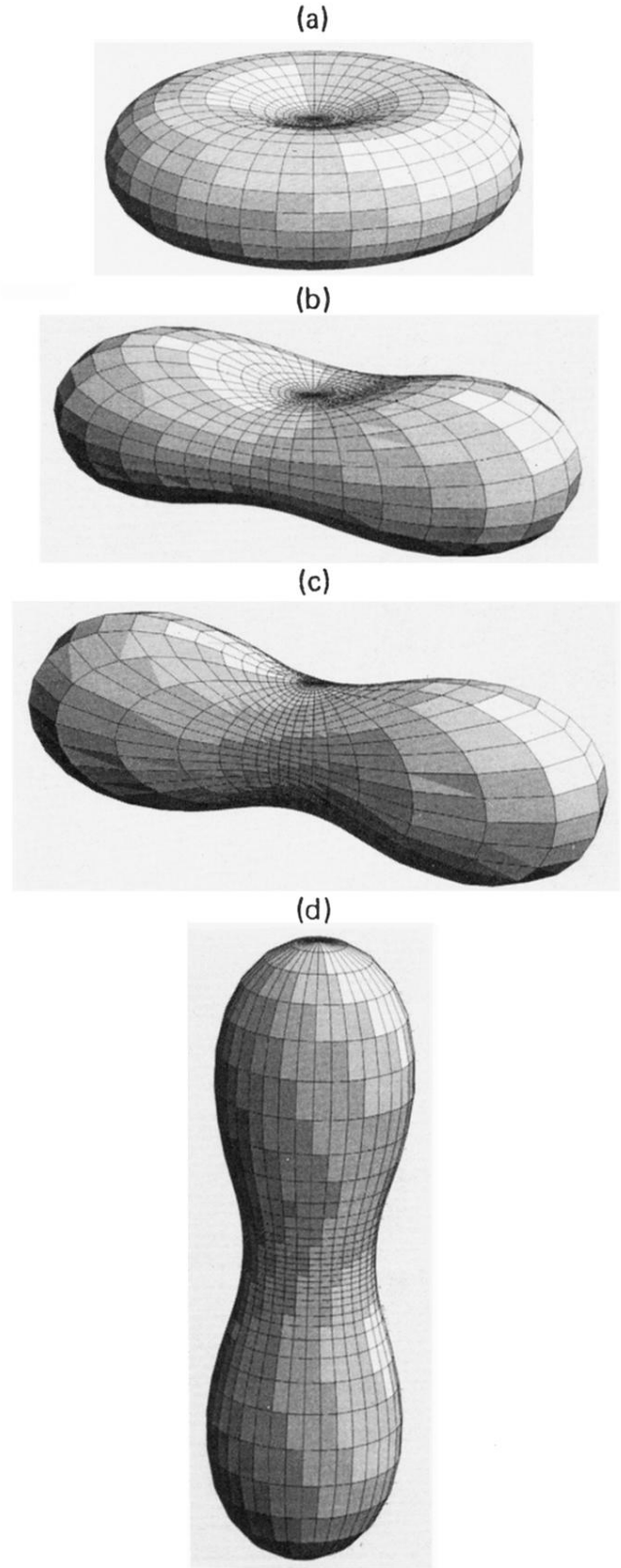

FIG. 2. Examples of stationary vesicle shapes obtained at $v_0 = 0.7$. Shapes (a), (c), and (d) are axisymmetric, where (c) and (d) represent the same dumbbell shape in different orientations with respect to the fixed reference frame. The two shapes (a) and (c,d) belong to the points M_1 and M_2, respectively [see Fig. 1(c)]. Shape (b) is a nonaxisymmetric intermediate shape between (a) and (c) corresponding to point M in Fig. 1(c).